Using 3D-Scene Data from a Mobile Detector System to Model Gamma-Ray Backgrounds

Marco Salathe, Mark S. Bandstra, Brian J. Quiter and Joseph C. Curtis

***Abstract*—Integration of contextual sensors into vehicle-borne mobile radiation detector systems delivers a rich description of the environment that could be used to estimate the complex and variable environmental gamma-ray backgrounds in urban areas. The predictions could potentially increase the sensitivity to illicit radiological and nuclear materials and could provide realistic inputs to urban radiological search simulations and algorithms. Recent work in this field has focused mainly on the predictive power of segmenting and classifying imagery from cameras and elected in its approach to aggregate the locations of gamma-ray interactions within the fielded detector array to a single point. This work builds upon the previous effort by leveraging LiDARs to create a 3D representation of the detector system and the surrounding scenery and demonstrates further improvement in the capability of attributing observed gamma-ray backgrounds to classes of surrounding materials.**

I. Introduction

THE Radiological Multi-sensor Analysis Platform (RadMAP) [1] was developed to investigate how contextual sensors can enhance radiological data. RadMAP carries a suite of radiation detectors and synchronized contextual sensors. A recent work [2] that was part of the Multi-agency Urban Search Experiment (MUSE) collaboration [3] has shown that panoramic videos can provide a semi-quantitative understanding of the sources of environmental radioactivity observed in gamma-ray detectors - particularly the array of 100 2”×4”×4” NaI(Tl) detectors. In addition to imagery generated by a pair of Ladybug3 cameras [4], RadMAP has fielded numerous additional contextual sensors, notably an inertial measurement unit (IMU) and LiDARs. The LiDARs produce 360 deg scans of the surrounding environment within their 30 deg opening angles every 0.1 s. The different scans can be used in Simultaneous Localization and Mapping (SLAM) to create a detailed spatial map of the entire facility and provide the exact location of the vehicle itself within that three-dimensional (3D) map. This eliminates some inherent constraints of the previous video-based analysis and allows a more complete description of the measured geometries throughout the radiological survey. The methods developed to leverage the 3D information, detector-specific sensitivity calculations, and gamma-ray energy specificity to algorithmically attribute measured gamma-rays to the surroundings are described here, along with some initial results.

Manuscript received December 13, 2019. This work was performed under the auspices of the US Department of Energy by Lawrence Berkeley National Laboratory under Contract DE-AC02-05CH11231. The project was funded by the US Department of Energy, National Nuclear Security Administration, Office of Defense Nuclear Nonproliferation Research and Development (DNN R&D). This research used resources of the National Energy Research Scientific Computing Center (NERSC), a U.S. Department of Energy Office of Science 55 User Facility operated under Contract No. DE-AC02-05CH11231.

M. Salathe, M. S. Bandstra, B. J. Quiter and J. C. Curtis are with the Applied Nuclear Physics Program at Lawrence Berkeley National Laboratory, Berkeley, CA 94720 USA. Email: msalathe@lbl.gov.

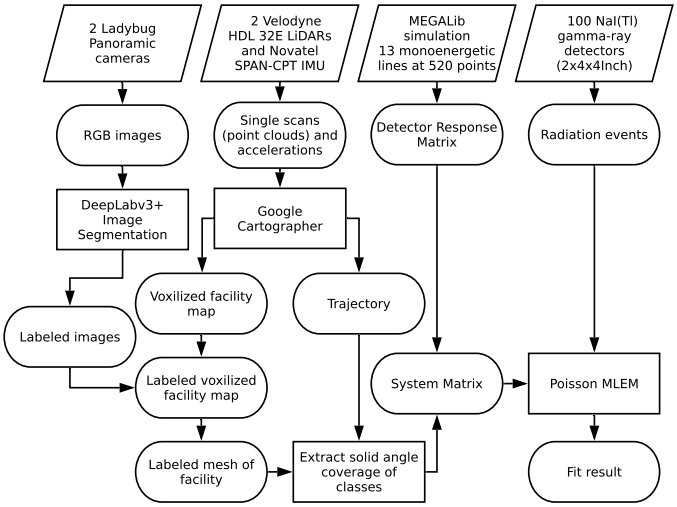

Fig. 1. A diagram of the analysis procedure. Parallelepipeds represent methods by which data are generated, round boxes represent intermediate data products, and rectangles represent analysis steps.

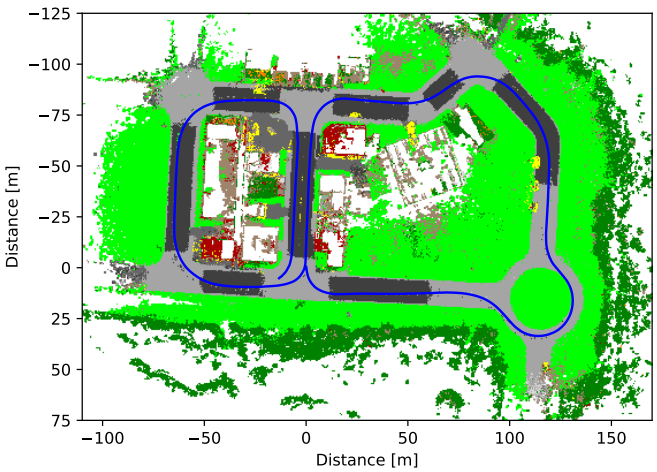

Fig. 2. A top down view on the labeled voxel-grid of the MOUT facility. The track of RadMAP is displayed in blue.

II. Methodology

This work will focus on measurements conducted at the Military Operations in Urban Terrain (MOUT) facility at the Fort Indiantown Gap (FTIG) National Guard Training Center, for which radiological ground truth data have been collected on site [5]. The examined sequence is limited to a 165 s long period of continuous motion of RadMAP and is identical to the one used in the previous study [2].

Google Cartographer [6] was used to perform SLAM on the LiDAR's scan data and acceleration vectors measured by the IMU to produce a temporal trajectory of the vehicle and a voxelized representation of the training facility. Hand labeled images from the Ladybug3 cameras were used to update the classifier weights of the pre-trained DeepLabv3+ [7] image segmentation neural network to distinguish features such as grass, forest, buildings, concrete, asphalt, etc. The retrained network was then used to segment the Ladybug3 camera images sampled at 3 Hz. The classified images were projected onto the voxelized map to segment it into the above mentioned classes. A top down view of the resulting voxel-grid colorized by each class is shown in Fig. 2. Finally, the resulting voxelized map was turned into a triangular mesh using an enhanced version of Open3D's [8] pivoting ball algorithm.

The spectral response of the detector modules was simulated in MEGAlib [9] for 13 monoenergetic far field gamma-ray sources at 520 points subtending the unit sphere. Through interpolation, a probability distribution of the gamma-ray energies emitted from each surface for any detected energy at all possible angles can be approximated. The field of view of each individual Na(Tl) gamma-ray detector at any given moment as RadMAP moves along its trajectory was extracted from the mesh to calculate the angular coverage of each image-derived material class.

A feature vector α_l encodes unknown aspects of the scene. In the most simple case it describes the areal radiation emission rate (emitted photon current) of each class, but can also encode spectral information. Here, each material class was divided in 119 equally sized energy bins to include spectral information. Probabilities of detecting gamma-rays associated with photon emissions comprise the system matrix R_l at timestamp t as a function of emitted (E) and detected (E'') energy given by:

$$R_l(t, E'', E) = \sum_{E',i} A_i(E''|E') S_{\text{air}}(E'|E, r_i(t)) \frac{\delta_{l,label(t,i)} \Delta\Omega_i}{\pi} \quad (1)$$

where S_{air} describes scattering in air – a function of the distance to a given surface $r_i(t)$. The effective area A_i describes the detector response of a given surface. The function $\delta_{l,label(t,i)}$ maps the coverage of a solid angle element $\Delta\Omega_i$ to the respective class. The sum over all solid angle elements should cover the entire unit sphere, thus elements that are obstructed by intervening materials are not considered in the above description.

The activity associated with the features can be calculated using the list-mode Poisson Maximum Likelihood Estimation Maximization (MLEM) update algorithm [10]:

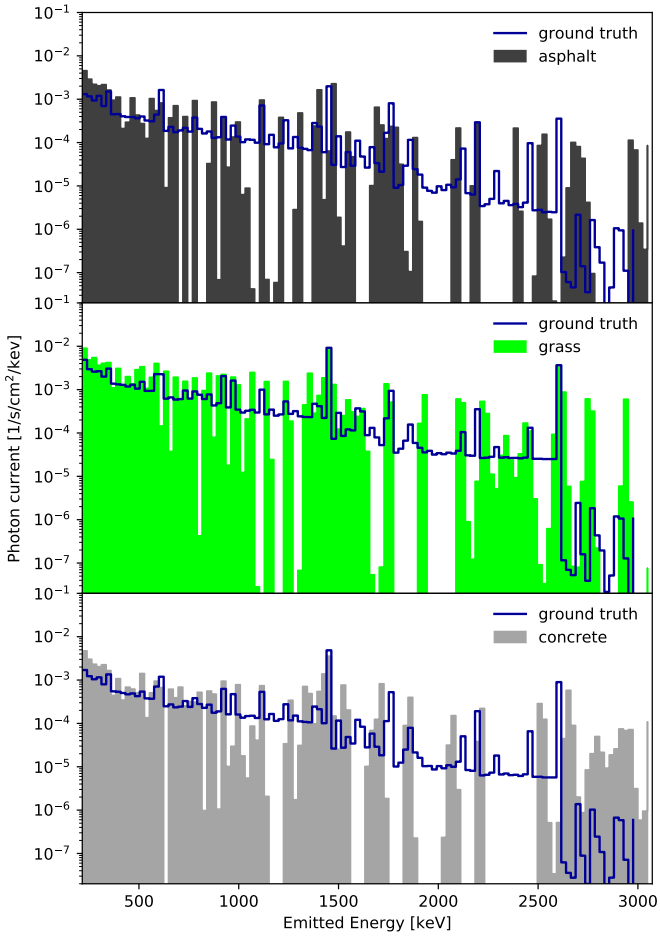

Fig. 3. The MLEM solution for the emitted photon currents of the three most prominent classes compared to the ground truth data from Ref. [5].

$$\alpha_l^{j+1}(E) = \frac{\alpha_l^j(E)}{S_l} \sum_n^N \frac{R_l(t_n, E_n'', E)}{\sum_{\tilde{l}} \alpha_{\tilde{l}}^j(E) R_{\tilde{l}}(t_n, E_n'', E)} \quad (2)$$

The sensitivity S_l is the integral of $R_l(t, E'', E)$ over time and the sum over the energies E and E''. The subscript n refers to a single gamma-ray detection of which there were approximately 2 millions measured during the 165 s long period.

III. Results

The list-mode MLEM analysis has been completed for the case where 119 energy bins – spanning energies of 216 to 3072 keV – were used as the feature vector for each class. The detectors have been all handled as individual modules, 13 of the 100 detectors were excluded due to poor energy resolution.

The resulting emission spectra are noisy and only the most prominent classes (shown in Fig. 3) express features that can be physically interpreted. The noisiness of the features is most likely caused by inaccuracies in the underlying model, such as an insufficient description of detector resolutions, the implicit assumption that each material class emits the same intensity and energy distribution of gamma rays, etc.

TABLE I

THE SUMMED PHOTON CURRENTS OF THE SPECTRAL FIT COMPARED TO THE GROUND TRUTH AND THE PREVIOUS WORK. THE DATA FROM [5] AND [2] WERE ADJUSTED TO REFLECT THE REDUCED ENERGY RANGE.

Class	Ground truth[5] [γ/s/cm^2]	Camera only[2] [γ/s/cm^2]	3D scene [γ/s/cm^2]
Asphalt	0.56	0.50±0.07	0.87
Concrete	0.69	0.74±0.04	1.01
Grass	1.68	1.58±0.04	2.60
Gravel	0.56	0.76±0.04	1.12
Building brown	0.31 / 0.47	0.71±0.02	0.90
Building red	0.28	0.83±0.02	0.98
Building white	0.22 / 0.36	0.70±0.04	0.98
Building roof	N/A	0.00±0.22	0.80
Forest	N/A	0.65±0.04	1.19
Vehicle	N/A	0.91±0.10	1.00
Sky	N/A	0.38±0.02	0.31
Poles	N/A	N/A	0.47

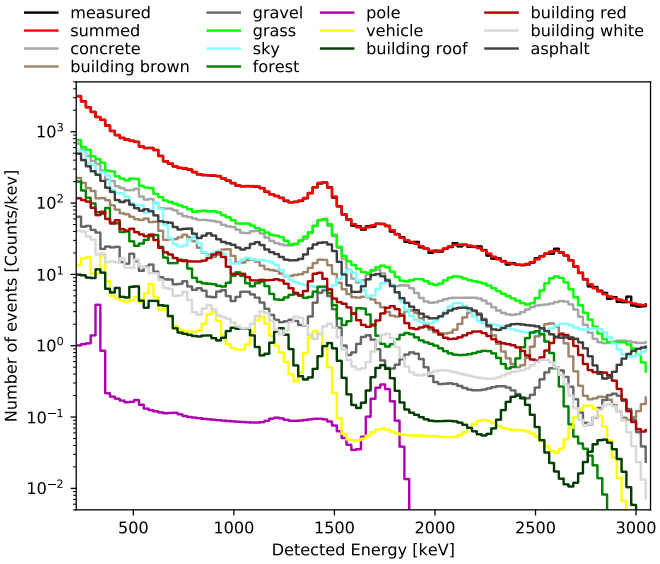

Fig. 4. The predicted number of counts in the detectors calculated by $\int \sum_E R_l(t, E'', E)\alpha_l(E)\mathrm{d}t$ due to each material class. The sum of the classes (red) is compared to the total measured spectrum (black).

By summing over all energies, one obtains the average photon current emitted by a given class listed in TABLE I. The ground truth currents were adjusted to only comprise the energy range between 216 and 3072 keV, the camera only value from [2] were compensated by multiplying them with a missing factor of 2 and removing 30%, the average in the range 0-216 keV of the ground truth spectra. The observed currents are mostly greater than those from the camera-only model of [2], which can be expected, as the camera only analysis did not include any scattering and attenuation in air. The currents also exceed the ground truth measurement by approximately 30%, but the relative amplitudes agree, suggesting that the fitted emission spectra indeed carry physical relevant information.

The predicted contribution of classes to the measured spectrum in the detectors (presented in Fig. 4) are calculated by multiplying the emission spectra with the system matrix and integrating over time. These spectra are less strongly effected by model inaccuracies and so physical peaks and a continuum

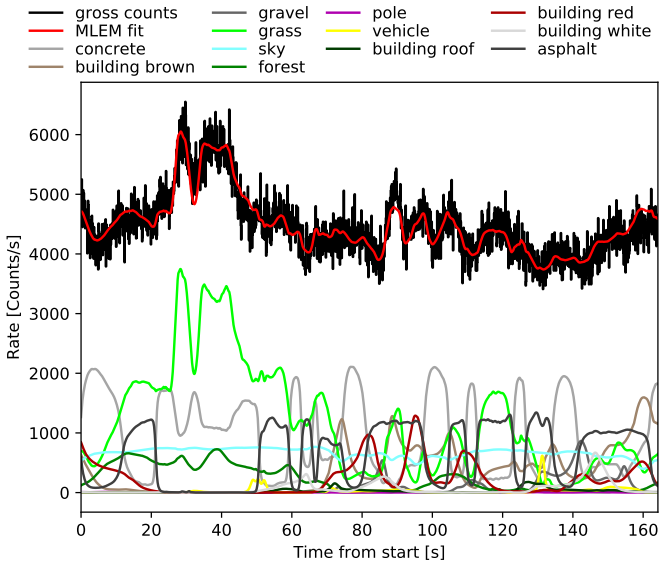

Fig. 5. The contribution of classes given by $\sum_{E'',E} R_l(t, E'', E) \cdot \alpha_l(E)$, the fit gross count rate obtained by summing all contributions from classes (red), and the measured gross count rate (black).

are visible. The sum over the individual contributions is in good agreement with the measured rate.

The temporal evolution of the detector array count rates due to the emitted photon current from each material class over the duration of the measurement is shown in Fig. 5. The summed contributions to the count rate follows the gross count rate observed in the detectors and the agreement is an improvement over the camera based model shown in Fig. 8 of [2].

IV. DISCUSSION

The knowledge about the spatial extent of the surrounding scene was used to match contributions of individual classes to gamma-ray event distributions observed in radiation detectors through list-mode MLEM. The resulting fit is an improvement over camera imagery only, suggesting incorporation of 3D information is valuable for associating observed gamma-ray activity with environmental sources. The inclusion of photon energy dependence to detection model enabled a direct comparison between spectra measured by RadMAP and those derived by summing those attributed to the various classes included in the MLEM model.

The next steps are to limit spectral features by postulating that the spectra emitted by each class can be described comprised as a sum of separate Thorium, Uranium and Potassium-induced radioactive emissions. The emission spectra for these elements can be simulated thus reducing the requirement for a unconstrained spectral fit. Reconstructing spectral activities for each material class, would demonstrate substantial understanding of the radiological environment that has only been achieved through very labor-intensive ground truth measurement campaigns.

REFERENCES

[1] M. S. Bandstra, T. J. Aucott, E. Brubaker, D. H. Chivers, R. J. Cooper, J. C. Curtis, J. R. Davis, T. H. Joshi, J. Kua, R. Meyer, V. Negut,

M. Quinlan, B. J. Quiter, S. Srinivasan, A. Zakhor, R. Zhang, and K. Vetter, "Radmap: The radiological multi-sensor analysis platform," *Nuclear Instruments and Methods in Physics Research Section A: Accelerators, Spectrometers, Detectors and Associated Equipment*, vol. 840, pp. 59 – 68, 2016.

[2] M. S. Bandstra, B. J. Quiter, J. C. Curtis, K. J. Bilton, T. H. Joshi, R. Meyer, V. Negut, K. Vetter, D. E. Archer, D. E. Hornback, D. E. Peplow, C. E. Romano, M. W. Swinney, T. L. McCullough, and M. L. McLean, "Attribution of gamma-ray background collected by a mobile detector system to its surroundings using panoramic video," *Nuclear Instruments and Methods in Physics Research Section A: Accelerators, Spectrometers, Detectors and Associated Equipment*, 2018.

[3] A. D. Nicholson, I. Garishvili, D. E. Peplow, D. E. Archer, W. R. Ray, M. W. Swinney, M. J. Willis, G. G. Davidson, S. L. Cleveland, B. W. Patton, D. E. Hornback, J. J. Peltz, M. S. L. McLean, A. A. Plionis, B. J. Quiter, and M. S. Bandstra, "Multiagency urban search experiment detector and algorithm test bed," *IEEE Transactions on Nuclear Science*, vol. 64, no. 7, pp. 1689–1695, July 2017.

[4] Point Grey Research Inc., *Ladybug3 Technical Reference Manual*, 1.8 ed., 12051 Riverside Way, Richmond, BC, Canada, 2011.

[5] M. W. Swinney, D. E. Peplow, B. W. Patton, A. D. Nicholson, D. E. Archer, and M. J. Willis, "A methodology for determining the concentration of naturally occurring radioactive materials in an urban environment," *Nuclear Technology*, vol. 203, no. 3, pp. 325–335, 2018.

[6] W. Hess, D. Kohler, H. Rapp, and D. Andor, "Real-time loop closure in 2d lidar slam," in *2016 IEEE International Conference on Robotics and Automation (ICRA)*, May 2016, pp. 1271–1278.

[7] L.-C. Chen, Y. Zhu, G. Papandreou, F. Schroff, and H. Adam, "Encoder-decoder with atrous separable convolution for semantic image segmentation," in *ECCV*, 2018.

[8] Q.-Y. Zhou, J. Park, and V. Koltun, "Open3D: A modern library for 3D data processing," *arXiv:1801.09847*, 2018.

[9] A. Zoglauer, R. Andritschke, and F. Schopper, "Megalib – the medium energy gamma-ray astronomy library," *New Astronomy Reviews*, vol. 50, no. 7, pp. 629 – 632, 2006, astronomy with Radioactivities. V.

[10] L. Parra and H. H. Barrett, "List-mode likelihood: EM algorithm and image quality estimation demonstrated on 2-D PET," *IEEE Transactions on Medical Imaging*, vol. 17, no. 2, pp. 228–235, April 1998.